ES Materials & Manufacturing

COMMUNICATION View Article Online

Fabrication of N, P-Codoped Mo_2C/Carbon Nanofibers Via Electrospinning as Electrocatalyst for Hydrogen Evolution Reaction

Pan Yang, Hexi Zhao, Yingnan Yang, Pengxiang Zhao, Xiaochong Zhao* and Lijun Yang*

Stable and efficient noble-metal-free electrocatalysts are imperative substitute of Pt-based electrocatalysts for hydrogen evolution reaction. In this study, N,P-codoped Mo_2C/carbon nanofibers prepared via electrospinning and one step heat treatment, exhibited a high dispersion of Mo_2C and existence of N and P, which benefit for the electrocatalytic performance of hydrogen evolution reaction. Solving ammonium phosphomolybdate hydrate (PMoHN) in precursor solution, Mo, N and P were introduced in carbon nanofibers, and dosage of PMoHN on electrocatalytic performance was investigated. Subsequently electrochemical tests reveal that 4% (wt. V^{1}) PMoHN shows the best catalytic performance. The overpotential under acidic (0.5 M H_2SO_4) and alkaline (1.0 M KOH) conditions are 196 and 107 mV to achieve the current density of 10 mA cm^{-2}, and Tafel slopes are 81.3 and 67.5 mV dec^{-1} respectively. Moreover, N, P-codoped Mo_2C/carbon nanofibers exhibits excellent stability under acidic and alkaline conditions.

Keywords: Electrospinning; Mo_2C; Carbon nanofiber; Hydrogen evolution reaction; Electrocatalysts

Received 29 November 2019, **Accepted** 8 January 2020

DOI: 10.30919/esmm5f618

1. Introduction

Hydrogen, as a clean, nontoxic, high-efficiency, friendly and recyclable resource, plays an important role in addressing the issue of environment pollution due to the combustion of fossil fuel.[1,2] At present, most of the hydrogen produced by reforming methane steam and coal gasification, which were not only energy consuming but also environment destruction.[3,4] In recent years, there has been an increasing interest in electrocatalysts for hydrogen evolution reaction (HER) for water splitting due to simpleness, efficiency and the high-purity hydrogen production. Generally, platinum (Pt)-based transition metal as the state-of-the-art catalysts for HER hinders large-scale application because of the high price, exiguity, and easy to poison.[5-7] It is imperative to develop the noble-metal-free electrocatalysts to substitute Pt-based catalysts. Among the noble-metal-free compound, with the similar d-band electron density state with Pt, molybdenum carbide (Mo_2C) -based materials have caused widely attention in HER because of their low cost, stability, corrosion resistance and excellent catalytic properties.[8,9] However, the poor conductivity and slow interfacial reaction kinetics hinder catalytic performance of Mo_2C.[10] The negative free energy of hydrogen adsorption (ΔG_{H^*}) of Mo_2C suggesting so strong Mo-H bonding on the surface of Mo_2C that H_2 was difficult to desorption.[11,12] In this regard, strategy of introduction of electron-rich element, such as N and P, could change the electron density to promote HER performance. Yang *et al* synthesized Mo_2C@C difunctional compound, which exhibited an excellent performance due to C enhance conductivity of the catalyst.[13] In addition, Ji *et al* synthesized N,P-Mo_xC nanoparticles, which exhibited a low overpotentials of 107 and 135 mV at 10 mA cm^{-2} in 0.5 M H_2SO_4 and 1.0 M KOH solution.[14]

Herein, N, P-Mo_2C/carbon nanofibers (CNF) electrocatalyst was prepared by electrospinning and one-step pyrolysis to accomplish large-scale production. Mo, N and P are incorporated in carbon nanofibers by solve ammonium phosphomolybdate hydrate (PMoHN) in precursor solution. Dosage of PMoHN on electrocatalytic performance is investigated. N, P-codoped Mo_2C/CNF catalyst exhibits proper electrocatalytic performance and excellent stability under

Institute of Materials, Chinese Academy of Engineering Physics, Jiangyou, China
***E-mail:** zhaoxiaochong@caep.cn (X. C. Zhao); sherry_yang0710@163.com (L. J. Yang)*

acidic and alkaline conditions.

2. Experimental section

2.1 Chemicals

Polyvinylpyrrolidone (PVP, M_w = 13, 00, 000) and polyacrylonitrile (PAN, M_w = 150,000) were purchased on Aladdin Reagent Co. Ltd., while ammonium phosphomolybdate hydrate ($(NH_4)_3PMo_{12}O_{41}\cdot xH_2O$, define x = 6 when calculating), N,N-dimethylformamide (DMF), absolute ethanol, sulfuric acid (H_2SO_4) and potassium hydroxide (KOH) were purchased on Sinopharm Chemical Reagent Co. Ltd. Pt/C (20 wt% loaded in carbon black) and Nafion (5 wt%) reagents were purchased from Alfa Aesar. The deionized water throughout all experiments was purified through Sartorius purity water system (resistivity of 18.2 MΩ·cm). All chemicals are analytical grade and used directly without further purification.

2.2 Synthesis of Mo_2C/CNFs

Firstly, PAN and PVP were dissolved in the 10 mL of DMF by stirring at 60 °C for 3 h to form 10 wt% PAN/PVP/DMF solution which contain the a 1:1 mass ratio of PAN to PVP. Then, 2 wt% Ammonium phosphomolybdate hydrate (PMoHN) was dissolved in the precursor solution by ultrasonication for 2 h and stirred at 60 °C for 12 h to obtain a dark green viscous homogeneous solution.

Finally, electrospinning and heat treatment: a free-type electrospinning machine was employed as electrospinning when the air humidity was about 50%, the applied voltage was 60 kV, and the aperture at the mobile liquid supply device was 0.6 mm. The distance between receiving plate (aluminum foil) and droplet was 25 cm. After electrospinning, the fiber was removed from the aluminum foil paper, placed in a clean porcelain boat, and heat-treated in a vacuum tube furnace. The heat treatment steps were as follows: (1) pre-oxidation in air at 250 ºC for 2 h, (2) stable treatment in Ar at 450 ºC for 2 h, (3) the carbonization treatment in Ar at 900 ºC for 2 h. To simplify the following discussion, the CNFs doped with PMoHN with weight percentages of 2%, 4% and 6% for electrospinning were signed as 2%-PMoHN-CNFs, 4%-PMoHN-CNFs and 6%-PMoHN-CNFs.

2.3 Structural analysis and morphological characterization

The morphology was characterized with scanning electron microscope (SEM, Hitachi S4800) and high-resolution transmission electron microscope (HR-TEM, SN8000). X-ray diffraction (XRD, Bruker D2 PHASER) was conducted on analyze the structure of the sample, using a continuous scanning method with Cu-K_α radiation. X-ray photoelectron spectroscopy (XPS, Escalab 250xi) were studied to analyze the valence of the samples.

2.4 Electrocatalytic performance test

3 mg sample and 40 μL Nafion was dispersed in 460 μL ethanol by ultrasonic for 2 h obtained a homogeneous ink. The working electrode was a 3 mm diameter glassy carbon electrode (GCE) polished before use. Take 5 μL of the above slurry on the surface of the GCE and tested it after air drying. The catalyst loading was 0.28 mg cm^{-2}.

The test was carried out at 20 °C using a Sartorius electrochemical test system. The electrolyte was degassed by nitrogen for 30 min before the test to remove dissolved oxygen. A three-electrode system was used with a platinum plate as the counter electrode and a saturated calomel electrode (SCE) as the reference electrode (corrected before use,[15] $E_{vs\ SCE}$ = 0.244 V). From the Nernst equation, the potential of the reversible hydrogen electrode (RHE) is $E_{vs\ RHE} = E_{vs\ SCE} + 0.0591 \times pH + iR$. The cathodic polarization curve (LSV) scan rate was 2 mV s^{-1} and was processed by activation before testing in 0.5 M H_2SO_4 and 1 M KOH. R is measured by electrochemical impedance spectrum (EIS) with a frequency range of 0.1 to 100 k Hz with an amplitude of 5 mV. The Tafel slope is a linear fit of the points in the Tafel region from the LSV plot using a linear fitting method. The stability of the catalyst was tested by measure *i-t* curve. The potential values of the curves are compensated for 95% iR, and all current densities are normalized by geometric area.

3. Results and discussion

The surface morphology and diameter of fiber can be obtained by SEM. As shown in Figs. 1a, c, e and g, the series of nanofibers show smooth surface and almost uniform diameter distribution, presenting a three-dimensional network structure. The diameter of CNFs is the largest (286 nm) followed by 2%-PMoHN-CNFs (232 nm), 6%-PMoHN-CNFs (219 nm) while the 4%-PMoHN-CNFs (216 nm) are the smallest. Meanwhile, CNFs and 2%-PMoHN-CNFs exhibit smooth surface, while the 4%-PMoHN-CNFs and 6%-PMoHN-CNFs show "cluster-like" protrusions phenomenon, which may be caused by Mo_2C nanoparticles of on surface of the fiber. 4%-PMoHN could be the best dosage for CNF due to the smallest diameter.

The elemental mapping was measured in order to verify the existence of the N, P, Mo element. Obviously, the element mapping shown in Fig. 2a reveals the uniform coexistence of Mo, N and P elements and successful synthesis of N, P-Mo_2C/CNF. As observed from Fig. 2b, the TEM image of 4%-PMoHN-CNFs suggested the Mo_2C has a uniform distribution in the shadow. It indicates that the binding of fibers could reduce the agglomeration of Mo_2C during calcination. In the Fig. 2c, the HR-TEM clearly highlight that Mo_2C particles are coated with layered graphitized carbon structures with a typical interplanar crystal spacing of 0.33 nm according to the PDF 26-1080. Meanwhile, HR-TEM shows the lattice fringes with an

interplanar crystal spacing of 0.23 and 0.24 nm closely match the (101) and (002) planes of β-Mo_2C according to the PDF 35-0787, respectively. The XRD analysis further proved that the result of final carbonized product is β-Mo_2C.

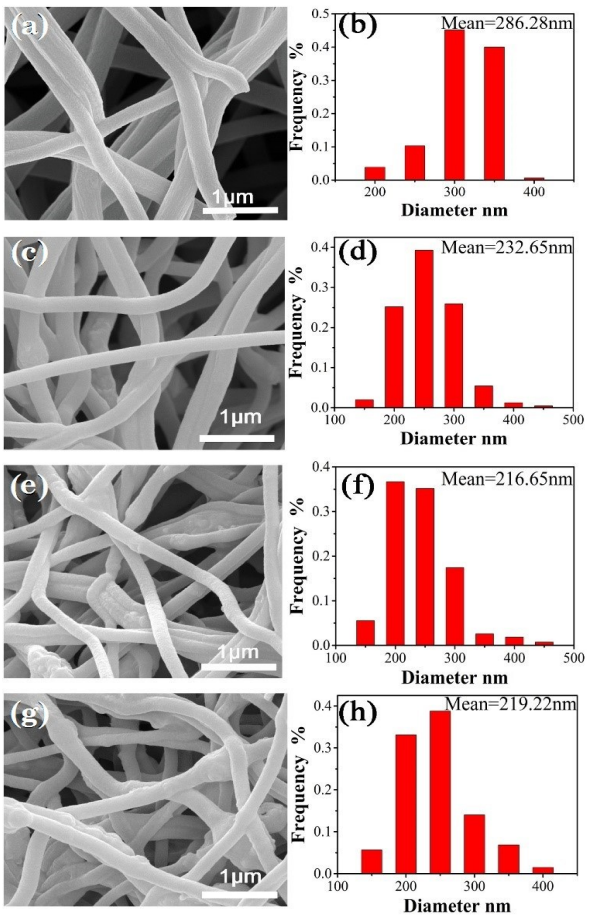

Fig. 1 SEM images and diameter distribution of samples: (a, b) CNFs; (c, d) 2%-PMoHN-CNFs; (e, f) 4%-PMoHN-CNFs; (g, h) 6%-PMoHN-CNFs.

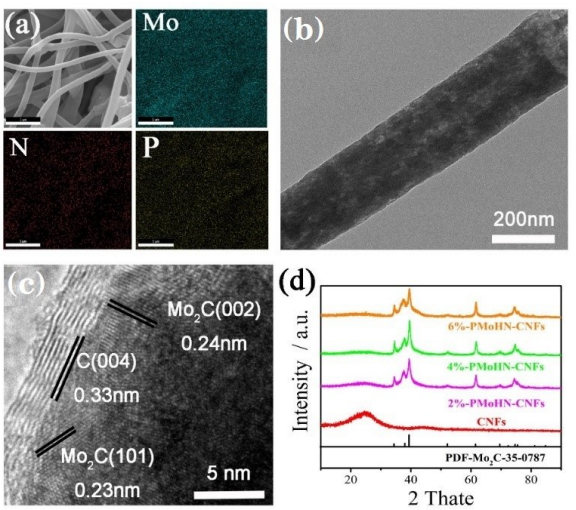

Fig. 2(a-c) SEM and element mapping, TEM and HRTEM of 4%-PMoHN-CNFs; (d) XRD patterns of 2%, 4%, and 6%-PMoHN-CNFs.

X-ray photoelectron spectroscopy (XPS) measurements were devoted to investigating the chemical elements and chemical valence state of 4%-PMoHN-CNFs. The survey spectra of sample in Fig. 3a display the signals of the elemental C, N, O, Mo and P, suggesting that N and P were successfully introduced into the 4%-PMoHN-CNFs.[14] As shown in Fig. 3b, Mo 3d display three characteristic states (+2, +4 and +6) for Mo_2C.[16] The peaks of Mo $3d_{5/2}$ and Mo $3d_{5/2}$ for Mo^{2+} at 228.0 and 231.2 eV should originate from Mo_2C. In addition, the partial surface oxidation of MoC_x in carbonization/air may be ascribed to the peaks of Mo^{4+} and Mo^{6+}.[17,18] In the N 1s XPS spectrum, as illustrated in Fig. 3c, the wide peak can be divided into five individual types of elements species, corresponding to Mo 3p (394.5 eV), Mo-N (396.6 eV) as well as pyridinic-N (398.2 eV), pyrrolic-N (400.2 eV) and graphitic-N (402.2 eV).[19] Obviously, the presence of C-N bond and Mo-N bond indicates that nitrogen-doped nanofibers and nitrogen-doped Mo_2C exist in 4%-PMoHN-CNFs which can be improve more active sites for HER. The doublet in the P 2p region (132.6 eV and 133.58 eV) can attributable to Mo-P in the Fig. 3d. While the peak at 136.9 eV and 138.3 eV corresponds to P-C and P-O banding.[14] Therefore, among P-Mo, N-Mo, C-N and C-P bonding, the XPS measurements demonstrate the possible N, P-doping in Mo_2C and CNF.

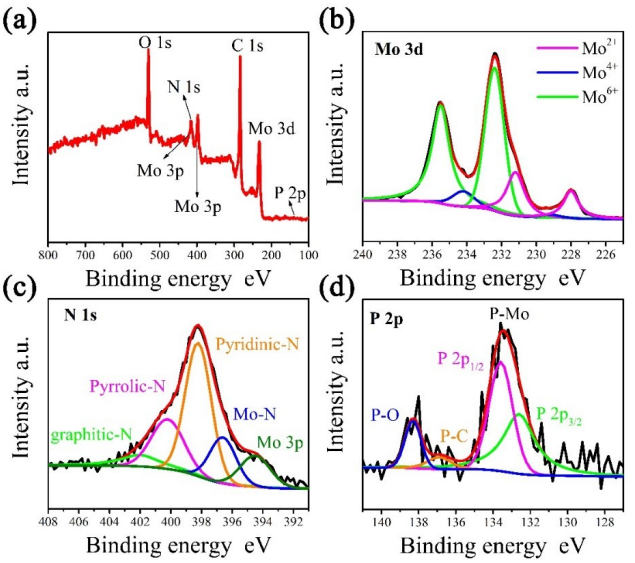

Fig. 3 XPS spectrum of 4%-PMoHN-CNFs.

LSV curve and Tafel slope are commonly investigated to evaluate the HER performance of catalyst. The cathode current density increases rapidly at a small overpotential, indicating that the synthetic has a higher catalytic activity and a smaller Tafel slope. As shown in Figs. 4a and b, 20 wt% Pt/C, a commercial HER catalysts for comparison, has the highest catalytic activity and the nearly zero onset potential. Since HER instrument with sun-light coupling usually works under the condition of 10~20 mA cm^{-2}, the overpotential on the

current density of 10 mA cm^{-2} is another important parameter for water-electrolysis.[20] It can be seen that 4%-PMoHN-CNFs requires the lowest overpotential (196 mV and 107 mV in acidic and alkaline conditions, respectively), compared to the 2%-PMoHN-CNFs (257 and 246 mV) and 6%-PMoHN-CNFs (224 and 142 mV), indicating that the optimum mass ratio of PMoHN is 4%.

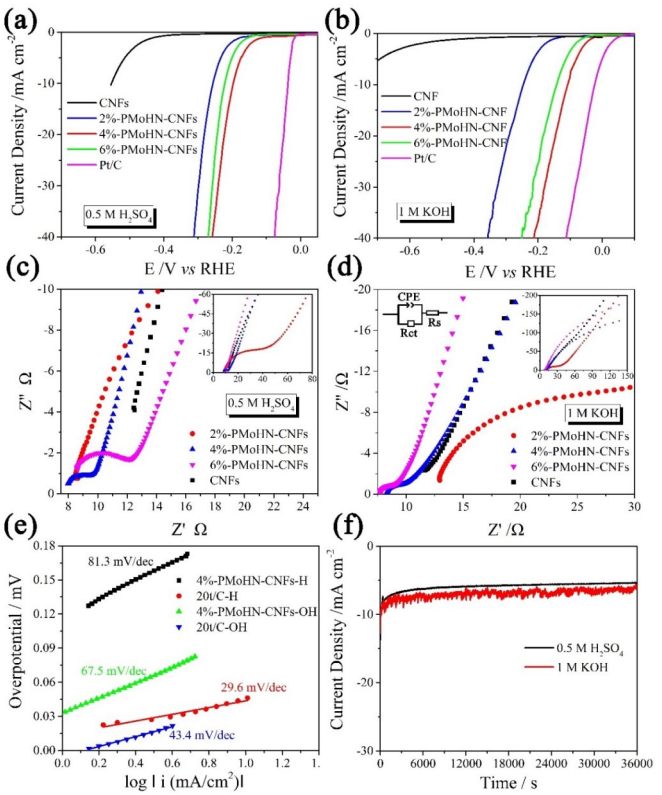

Fig. 4 Electrochemical test results for samples. (a, b) LSV plots of samples in 0.5 M H_2SO_4 and 1 M KOH solution; (c, d) Nyquist plot of samples in 0.5 M H_2SO_4 and 1 M KOH solution, the inset is the original Nyquist plot; (e) Tafel slope of 4%-PMoHN-CNFs-X and 20% Pt/C-X (X is in 0.5 M H_2SO_4 and 1 M KOH solution); (f) *i-t* plot of 0.50% C_3N_4 CNFs in 0.5 M H_2SO_4 and 1 M KOH solution.

The equivalent circuit diagram (inset of the Fig. 4d) is composed of charge transfer resistance (R_{ct}), solution resistance (R_s) and constant phase element (CPE) to fit the electrochemical impedance spectroscopy (EIS) results of the catalyst. The semicircle in the high frequency region corresponding to the charge transfer resistance R_{ct} can reflect the kinetics of the electrocatalyst which a lower R_{ct}value represents a faster reaction rate.[21] The EIS shows that the R_{ct} value of synthesis is consistent with the LSV performance (Fig. 4c and d).

The Tafel slope is generally evaluated the catalytic performance and mechanism of the HER catalyst. A smaller Tafel slope generally means that the electrocatalyst requires a lower overpotential to achieve the desired current density. The catalytic mechanism generally has as following classical theories:[22]

Volmer-Tafel Mechanism of HER (Tafel slope = 30~40 mV dec^{-1}):

$H^+(aq) + * + e^- \rightarrow 2H^*$ (adsorption and discharge of proton)

$2H^* \rightarrow H_2(g) + 2^*$ (chemical desorption of H_2)

Volmer-Heyrovsky Mechanism of HER (Tafel slope = 50~120 mV dec^{-1}):

$H^+(aq) + * + e^- \rightarrow 2H^*$ (adsorption and discharge of a proton)

$H^* + H^+(aq) \rightarrow H^* - H^+$ (adsorption of another proton on the same site)

$H^* - H^+ + e^- \rightarrow H_2(g) + *$ (discharge and desorption of H_2)

Fig. 4e shows the Tafel slope value of the catalyst in 0.5 M H_2SO_4 solution. The commercial 20 wt% Pt/C has a Tafel slope of 29.6 mV dec^{-1} in acidic condition, which is a typical Volmer-Tafel reaction. The Tafel slope of 4%-PMoHN-CNFs is 81.3 and 67.5 mV dec^{-1} in acidic and alkaline conditions, indicating that Volmer – Heyrovsky reaction was taken as the catalytic mechanism.

Long-term stability performance is one of the important parameters of the HER catalyst. It can be seen from Fig. 4f that the current density little decrease after 10 h test, indicating that the catalyst has good catalytic stability in acidic and alkaline electrolytes. Table 1 summarizes some of the reported literatures on the catalytic performance of some non-metallic catalysts. From this table, the materials of this study have lower overpotential and electrospun method, indicating better HER catalytic performance and large-scale production.

Overall, the superior HER performance of 4%-PMoHN-CNFs is attributed to several features. i) The well-dispersed nanofiber provides ample and available catalytically active sites. ii) The N,P-codoping Mo_2C and CNFs can improve the rich-electron and delocalization properties to increase the active sites and reaction energy barrier for HER.[23]

4. Conclusion

In a word, this paper reported a large-scale approach for fabrication of doped N, P doped Mo_2C-CNFs as an abundant and accessible active catalyst with a low cost via electrospinning and carbonization for highly HER performance. The synthesis with an optimal dosage of PMoHN (4%) possesses a high catalytic activity which is embodied in the overpotential is 196 and 107 mV at 10 mA cm^{-2} in 0.5 M H_2SO_4 and 1.0 M KOH. In addition, 4%-PMoHN-CNFs exhibited a prominent long-term stability after 10 h. In summary, this work demonstrates the low cost, large scale manufacture of electrocatalysts with the potential to apply to the industrial catalysis.

Table 1 HER catalytic properties of the partially reported non-metallic element catalyst.

Catalysts	η@10 (mV)	Tafel slope (mV dec^{-1})	Mass loading (mg cm^{-2})	Electrolyte	Method	Ref.
N,P-Mo_xC-NF	107	65.1	GCE@0.212	0.5 M H_2SO_4	Facile interfacial polymerization method and pyrolysis	(14)
	135	57.1		1 M KOH		
Ni/Mo_2C-NCNFs	143	57.8	GCE@1.4	1 M KOH	Electrospun and thermal treatment	(10)
Mo_2C@GO	152	65		0.5 M H_2SO_4	Chemical vapor deposition	(25)
	121	54		0.1 M KOH		
Mo_2C@NC	60	60	GCE@0.28	0.5 M H_2SO_4	Situ synthesis and one-step thermal treatment	(26)
	65	-		1 M KOH		
MoO_3/C-Mo_2C/C	175	66	GC@1.0	0.5 M H_2SO_4	Liquid-phase selfassembly reaction and thermal treatment	(27)
	≈125	63		1 M KOH		
Co-Mo_2C@NCNT	186	79	GCE@0.35	1 M KOH	Two heat treatments	(28)
NP-Mo_2C	210	64	GCE@0.21	0.5 M H_2SO_4	Precipitation and thermal treatment	(29)
Ni/Mo_2C-Porous Carbon	179	101	GC@0.5	1 M KOH	Hydrothermal method and thermal treatment	(30)
Mo_2C@C	180	71	GCE@0.28	0.5 M H_2SO_4	Templates and hermal treatment	(31)
	125	72		1 M KOH		
N,P- Mo_2C@C	141	56	GCE@0.9	0.5 M H_2SO_4	Simple polymerization and carbothermal reduction	(9)
	47	71		1 M KOH		
N,P-Mo_2C-CNF	196	81.3	GCE@0.28	0.5 M H_2SO_4	Electrospun and thermal treatment	This work
	107	67.5		1 M KOH		

η@10: Overpotentials at current density of 10 mA cm^{-2}
GCE: Load in glassy carbon electrode
GC: Load in glassy carbon disk electrode

Acknowledgement

This work is funded in part by the National Natural Science Foundation of China (No. 51602293) and the Key Research and Development Plan of Sichuan Province (No. 2018GZ0515).

Conflict of interest

There are no conflicts to declare.

References

1. T. N. Veziroğlua and S. Şahi'n, *Energ. Convers. Manage.*, 2008, **7**, 1820-1831.
2. S. Dunn, *Int. J. Hydrogen Energy*, 2002, **27**, 235-264.
3. P. Jiang, J. Chen and C. Wang, *Adv. Mater.,* 2018, **30**, 1705324.
4. W. Ahn, M. G. Park, D. U. Lee, M. H. Seo, G. Jiang, Z. P. Cano, F. M. Hassan and Z. Chen, *Adv. Funct. Mate*r., 2018, **28**, 1802129.
5. H. Zhang, L. Yu, T. Chen, W. Zhou and X. W. Lou, *Adv. Funct. Mater.*, 2018, **28**, 1807086.
6. J. Chen, J. Liu, J. Q. Xie, H. Ye, X. Z. Fu, R. Sun and C. P. Wong, *Nano Energy*, 2019, **56**, 225-233.
7. C. Wu, D. Liu, H. Li and J. Li, *Small*, 2018, **14**, 1704227.
8. W. Han, L. Chen, B. Ma, J. Wang, W. Song, X. Fan, Y. Li, F. Zhang and W. Peng, *J. Mater. Chem. A,* 2019, **7**, 4734-4743.
9. Y. Y. Chen, Y. Zhang, W. J. Jiang, X. Zhang, Z. Dai, L. J. Wan and J. S. Hu, *ACS Nano*, 2016, **10**, 8851-8860.
10. M. Li, Y. Zhu, H. Wang, C. Wang, N. Pinna and X. Lu, *Adv. Energy Mater.*, 2019, **9**, 1803185.
11. T. T. Yang and W. A. Saidi, *Nanoscale*, 2017, **9**, 3252-3260.
12. Z. Shi, K. Nie, Z. J. Shao, B. Gao, H. Lin, H. Zhang, B. Liu, Y. Yang, Y. Zhang, X. Sun, X. M. Cao, P. Hu, Q. Gao and Y. Tang, *Energy Environ. Sci.*, 2017, **10**, 1262-1271.
13. Y. Huang, Q. Gong, X. Song, K. Feng, K. Nie, F. Zhao, Y. Wang, M. Zeng,

J. Zhong, Y. Li, *ACS Nano*, 2016, **10**, 11337-11343.
14. L. Ji, J. Wang, X. Teng, H. Dong, X. He and Z. Chen, *ACS Appl. Mater. Interfaces*, 2018, **10**, 14632-14640.
15. R. Silva, D. Voiry, M. Chhowalla and T. Asefa, *J. Am. Chem. Soc.*, 2013, **135**, 7823-7826.
16. Y. Qiu, Z. Wen, C. Jiang, X. Wu, R. Si, J. Bao, Q. Zhang, L. Gu, J. Tang and X. Guo, *Small*, 2019, **15**, 1900014.
17. H. Yan, Y. Xie, Y. Jiao, A. Wu, C. Tian, X. Zhang, L. Wang and H. Fu, *Adv. Mater.*, 2018, **30**, 1704156.
18. Q. Liang, H. Jin, Z. Wang, Y. Xiong, S. Yuan, X. Zeng, D. He and S. Mu, *Nano Energy*, 2019, **57**, 746-752.
19. T. Ouyang, Y. Q. Ye, C. Y. Wu, K. Xiao and Z. Q. Liu, *Angew. Chem. Int. Ed.*, 2019, **58**, 4923.
20. S. Jing, L. Zhang, L. Luo, J. Lu, S. Yin, P. K. Shen and P. Tsiakaras, *Appl. Cataly. B: Environ.*, 2018, **224**, 533-540.
21. M. Chhetri, S. Maitra, H. Chakraborty, U. V. Waghmare and C. N. R. Rao, *Energy Environ. Sci.*, 2016,**9**, 95-101.
22. S. Anantharaj, S. R. Ede, K. Karthick, S. S. Sankar, K. Sangeetha, P. E. Karthik and S. Kundu, *Energy Environ. Sci.*,2018, **11**, 744-771.
23. R. Zhang, X. Wang, S. Yu, T. Wen, X. Zhu, F. Yang, X. Sun, X. Wang and W. Hu, *Adv. Mater.*, 2017, **29**, 1605502.
24. M. Zhang, S. S. Wang, T. Li, J. D. Chen, H. Zhu and M. L. Du, *Electrochim. Acta*, 2016, **208**, 1-9.
25. X. Fan, Y. Liu, Z. Peng, Z. Zhang, H. Zhou, X. Zhang, B. I. Yakobson, W. A. Goddard, X. Guo, R. H. Hauge and J. M. Tour, *ACS Nano*,2017, **11**, 384-394.
26. Y. Liu, G. Yu, G. D. Li, Y. Sun, T. Asefa, W. Chen and X. Zou, *Angew. Chem.*, 2015, **54**, 10752-10757.
27. C. Wang, L. Sun, F. Zhang, X. Wang, Q. Sun, Y. Cheng and L. Wang, *Small*, 2017, **13**, 1701246.
28. L. Ai, J. Su, M. Wang and J. Jiang, *ACS Sustainable Chem. Eng.*,2018, **6**, 9912-9920.
29. D. Wang, T. Liu, J. Wang and Z. Wu, *Carbon*, 2018, **139**, 845-852.
30. Z. Y. Yu, Y. Duan, M. R. Gao, C. C. Lang, Y. R. Zheng and S. H. Yu, *Chem. Sci.*, 2017, **8**, 968-973.
31. C. Wu and J. Li, *ACS Appl. Mater. Interfaces*,2017, **9**, 41314-41322.